Annals of Biomedical Engineering, Vol. 25, pp. 190–203, 1997
Printed in the USA.

0090–6964/97 $10.50 + .00

A Probabilistic Approach to Measure the Strength of Bone Cell Adhesion to Chemically Modified Surfaces

ALIREZA REZANIA, CARSON H. THOMAS, and KEVIN E. HEALY

Division of Biological Materials, Northwestern University Dental School, Chicago, IL, and Department of Biomedical Engineering, Robert R. McCormick School of Engineering and Applied Science, Northwestern University, Evanston, IL

Abstract—Patterned surfaces with alternating regions of amino silanes [*N*-(2-aminoethyl)-3-aminopropyl-trimethoxysilane (EDS)] and alkyl silanes [dimethyldichlorosilane (DMS)] have been used to alter the kinetics of spatial distribution of cells *in vitro*. In particular, we have previously observed the preferential spatial distribution of bone cells on the EDS regions of EDS/DMS patterned surfaces (10). In this study, we examined whether the mechanism of spatial distribution of cells on the EDS regions was adhesion mediated. Homogeneous layers of EDS and DMS were immobilized on quartz substrates and characterized by contact angle, X-ray photoelectron spectroscopy, and spectroscopic ellipsometry. The strength of bone cell attachment to the modified substrates was examined using a radial flow apparatus, within either 20 min or 2 hr of cell incubation in the presence of serum. A Weibull distribution was chosen to characterize the strength of cell-substratum adhesion. Within 20 min of cell exposure, the strength of adhesion was significantly larger on EDS and clean surfaces, compared with DMS surfaces ($p < 0.001$). Within 2 hr of cell incubation, there was no statistical difference between the strength of cell adhesion to EDS, DMS, and clean surfaces. The results of this study suggest that the surface chemistry mediates adhesion-based spatial cell arrangement through a layer of adsorbed serum proteins.

Keywords—Surface chemistry, Shear stress, Weibull distribution, Patterned surface chemistry, Tissue engineering.

INTRODUCTION

Chemical modifications of biomaterial surfaces have been extensively used to regulate the behavior or proteins and cells at interfaces. In particular, the promotion or prevention of cell adhesion to materials and medical devices has been a central objective in biomaterials research for over 25 years (1). A common direction in biomaterials research is that a better understanding of the mechanisms of cell adhesion to material surfaces may provide insights to new approaches in surface modification and implant design. In an effort to engineer specificity into biomaterial surfaces and enhance tissue compatibility at the site of implantation, tow forms of surface modification have shown significant promise: immobilization of organosilanes and alkanethiols with different terminal functionalites (9), and adsorption of extracellular matrix glycoproteins and synthetic peptide sequences to model biomaterial surfaces (12). For example, Sukenik *et al.* (27) showed that modification of titanium and glass substrates with organosilanes can modulate the functionality of fibronectin and the response of neuroblastoma cells to the surface. Furthermore, synthetic peptides containing sequences found within the cell binding domain of extracellular matrix proteins, such as Arg-Gly-Asp-Ser, have been grafted on silane-modified glass and polystyrene films, and were effective in enhancing cell spreading and adhesion (17).

The surface chemistry of a material can also be tailored to dictate the spatial distribution and morphology of mammalian cells *in vitro*. Photolithographic techniques, similar to the ones used in the semiconductor industry, have been used to modify biomaterial surfaces with controlled two-dimensional patterns, and guide cell organization and morphology (9,16). (In this study, we use the term "cell organization" to describe the spatial distribution of cells according to the underlying material surface chemistry. Materials with patterned surface chemistries offer cells either two or more regions with different functional groups exposed. Therefore, the use of patterned surface chemistry allows the examination of differential attachment of cells and protein adsorption under the same environmental conditions.

Despite the observed influence of surface chemistry and adsorbed serum macromolecules on cell organization, the mechanisms that govern the spatial distribution of cells in two dimensions are poorly understood. Kleinfeld *et al.* (13) used photolithography and silane chemistry to create two-dimensional patterned substrates to guide spinal and cerebellar cell organization on amine regions of amine/

Acknowledgment—Helpful discussions with Drs. E. P. Lautenschlager, M. DiMuzio, and A., Veis were gratefully appreciated. This research was supported by the national Institutes of Health/National Institute of Dental research (Grants T32-DE07042 and R03-DE10264) and by the National Institutes of Health/National Institute of Arthritis and Musculoskeletal and Skin Diseases (Grant R01-AR43187).

Address correspondence to Kevin E. Healy, Division of Biological Materials, Northwestern University, 311 East Chicago Avenue, Chicago, IL 60611-3008, U.S.A.

(Received 26Sep95, Revised 17Jan96, Revised 12Mar96, Accepted 25Mar96)

hydrophobic patterns in the presence of serum. In the absence of serum the cells did not organize according to the underlying chemistry of the surface. Recently, patterns of parallel lines with alternating surface chemistry have been used to control the organization and differentiation of primary bone cells in the presence of serum. It was found that, within 30 min of cell exposure to a patterned surface of amino- and alkylsilanes, there was preferential bone cell organization on aminosilane regions in the presence of serum or preadsorbed serum proteins (10) (see Fig. 1). Spectroscopic ellipsometry results indicated that the thickness of adsorbed protein layers from serum on alkyl- and aminosilane surfaces were not statistically different. From these observations, three possible factors deemed responsible for cell organization were proposed: (a) the type or density of adsorbed adhesive glycoproteins were different on alkylsilane and aminosilane surfaces; (b) the conformations of adsorbed proteins were different on the amino and alkyl silane modified surfaces; and (c) the density of "nonadhesive" proteins was greater on the hydrophobic, alkylsilane surfaces, compared with the hydrophilic surfaces (22,23). These studies indicate that, in addition to the chemistry of the patterned regions, environmental conditions (such as the presence of serum and secretion of microexudates by cells) modulate spatial distribution of cells.

In this study, we expand on our previous findings and test the hypothesis that the preferential organization of cells on aminosilane regions on a patterned substrate of aminosilane/alkylsilane is adhesion mediated. To test this hypothesis, a cell adhesion assay was used to estimate the strength of normal rat osteoblast attachment on homogeneous quartz surfaces modified with either an alkylsilane or aminosilane. The objectives of this investigation were to develop this cell detachment assay, introduce a novel probabilistic approach to analyze cell detachment data, and use the results of this method to further understand our previous cell patterning observations. The strength of bone cell attachment on modified quartz substrates was examined using a radial flow apparatus (RFA) (3). The advantage of the RFA over other cell adhesion apparatuses (such as parallel-plate and cone-plate) is that the RFA exposes a population of cells to a range of shear stresses, in a single experiment, thus generating a large number of data points (*i.e.*, number of detached cells *versus* shear stress). Due to the heterogeneity in the strength of cell attachment, possibly caused by differences in size and shape of attached cells, probabilistic and deterministic approaches were used to analyze cell-substratum adhesion strengths. Reverse sigmoidal, reverse log–normal, and three-parameter Weibull distributions were used to examine the effect of surface chemistry on the strength of bone cell adhesion to modified quartz surfaces. Results were analyzed to determine whether or not cell organization on patterned surfaces was adhesion mediated.

MATERIALS AND METHODS

Surface Preparation

All of the chemicals, except the organosilanes, were purchased from Aldrich (Milwaukee, WI, U.S.A.). The organosilanes were purchased from Hüls America (Piscataway, NJ, U.S.A.). Quartz discs (Quartz Scientific, Inc., Fairport Harbor, OH, U.S.A.) were cleaned ultrasonically for 10 min with ASTM grade I water [resistivity: 18 MΩ-cm, further referred to in this study as ultrapure water (UPW)], acetone, hexane, and etched in 9:1 (v:v) sulfuric acid:hydrogen peroxide for 15 min, rinsed in UPW, air-dried, and exposed to an oxygen plasma (March Plasmod, Concord, CA, U.S.A.) set at 0.5 mm Hg pressure and 100 W power for 5 min. Polished silicon wafers (*n* type, ⟨100⟩, International Wafer Service, Portola Valley, CA, U.S.A.), were used for spectroscopic ellipsometry and were processed in an identical manner as the quartz samples. All samples were dried in a laminar flow fume hood (class 100) and then stored in a desiccator until further analysis.

An amino silane [*N*-(2-aminoethyl)-3-aminopropyl-trimethoxysilane (EDS)] was bound to substrates using modifications to methods published elsewhere (10). Briefly, monolayers were prepared by immersing the substrates for 5 min in a solution of 1% EDS, 94% anhydrous methanol (1 mM acetic acid in methanol), and 5% UPW. Samples were then rinsed 3 times with methanol and oven-baked at 120°C for 5 min. Dimethyldichlorosilane (DMS) was immobilized on substrates by immersing in 5% DMS (0.41 M) in chlorobenzene for 5 min, followed by a rinse in chlorobenzene. All of the silane solutions were prepared in a glove box (nitrogen atmosphere) and transferred to a laminar flow fume hood for sample immersion, rinsing, and drying. After organosilane immobilization, the surfaces were characterized using contact angle, X-ray photoelectron spectroscopy (XPS), and spectroscopic ellipsometry (SE). Details of contact angle, XPS, SE measurements, and their results are described elsewhere (10). Briefly, the clean and EDS surfaces were hydrophilic, whereas the DMS surfaces were hydrophobic. SE results indicated a monolayer coating of EDS and a multilayer coating of DMS. XPS results also confirmed the presence of a DMS multilayer and an EDS monolayer on the surfaces. High-resolution XPS spectra of the EDS layer indicated the presence of a protonated amine ($—NH_3^+$) and a free amine ($—NH_2$), with relative amounts of 40 and 60%, respectively.

Cell Culture

Bone cells were isolated from calvaria of 6- to 12-day-old rats (Sprague-Dawley; Harlan, Indianapolis, IN, U.S.A.) and were cultured as previously described (10). Cells were maintained in 75 cm^2 flasks with 15% heat-

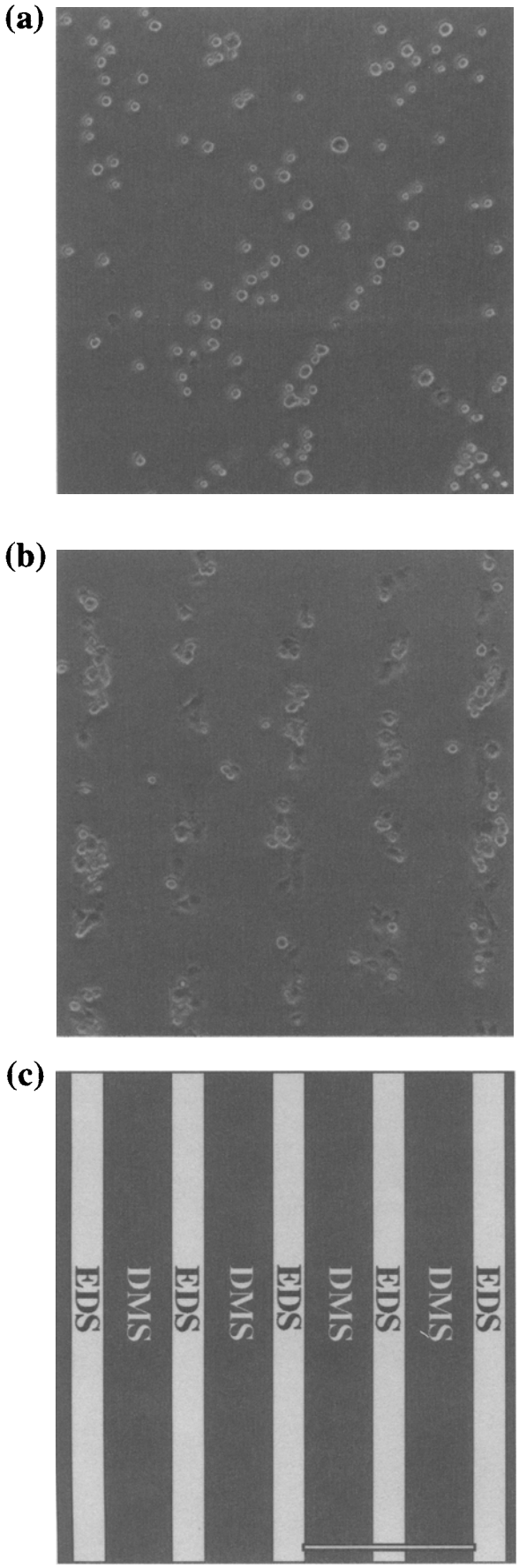

inactivated fetal bovine serum (FBS), 1% penicillin-streptomycin, 1% fungizone, HEPES buffer (15 mM), sodium pyruvate (1 mM), and ascorbic acid (5 μg/ml) in Dulbecco's modified Eagle's medium [(DMEM) Gibco, Grand Island, NY, U.S.A.)]. For the adhesion assay, cells at passage 2–4 were removed from flasks by exposure to 0.5 mM ethyleneglycol-*bis*-(β-aminoethyl)-*N,N,N',N'*-tetraacetoxymethyl (EGTA) for 10 min. Cell suspension in EGTA was then spun down at 4,000 rpm for 5 min and resuspended in DMEM with 15% heat-inactivated FBS. Cells were then plated on the appropriate quartz discs at a density of ~1×10^4 cells/ml (~5×10^3 cells/cm^2). The cell population used were verified to be osteoblast rich by positive staining for membrane-bound alkaline phosphatase and mineralized tissue (Von Kossa) (10).

Flow Chamber

The adhesive nature of modified surfaces was measured by an *in vitro* assay using the RFA. A schematic of the flow chamber is shown in Fig. 2. The flow chamber consists of (a) an upper quartz disc (6.3 cm × 0.32 cm) with cells attached, (b) a lower quartz disc (7.6 cm × 0.32 cm) with a 0.32 cm inlet hole at the center of the disc, (c) three 0.022-cm-thick glass spacers used to separate the upper and lower quartz discs, (d) an upper aluminum cover plate (10.5 cm × 0.63 cm) with a 5.4 cm hole at the center of the plate, (e) an aluminum base plate (10.5 cm × 0.63 cm) with a 6-cm hole at the center of the base, and (f) three Viton O-rings (Scientific Instruments Services, Inc., Ringoes, NJ, U.S.A.) were used to provide a good seal between the cover plate and the base. Outlet flow was through a 0.32-cm hole in the base plate. The flow assembly was placed on the stage of an inverted microscope (Nikon Diaphot, Tokyo, Japan). A rheoscopic fluid (Kalliroscope Corporation, Groton, MA, U.S.A.) was used to observe and confirm the presence of well-defined axisymmetric currents between the upper and lower quartz discs.

Cell Adhesion Measurements

A sterilized (immersed in 70% ethanol for 15 min) quartz sample (clean or silane treated) was plated with the cells for either 20 min or 2 hr in the presence of 15% FBS in DMEM at 37°C in an incubator. Subsequently, the sample was removed from cell suspension and placed in the flow chamber. While placing the sample in the flow

FIGURE 1. Rat calvaria bone cells on aminosilane/alkylsilane patterns. In the presence of serum, the bone cells preferentially attached to the aminosilane (EDS) regions. Within 5 min of cell exposure (a), cells were round and no cell organization was observed. Within 30 min (b) cell exposure, the bone cells preferentially spread and attached on the EDS regions. The EDS regions were 50 μm wide and the alkylsilane (DMS) regions were 100 μm wide (c). Scale bar, 250 μm.

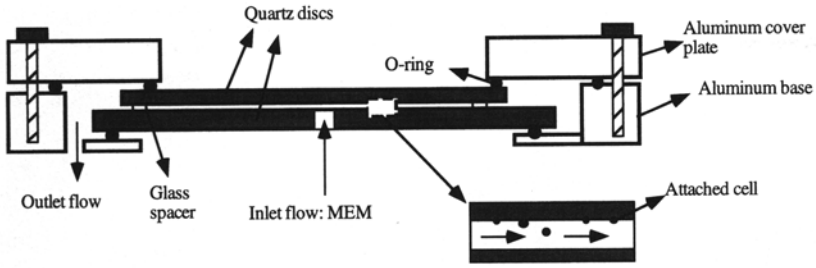

FIGURE 2. Schematic of the radial flow assay.

chamber, care was taken to keep disruption of the cells to a minimum. The flow chamber was then connected to a reservoir containing Minimum Essential Media (α-MEM; without FBS). The reservoir's temperature was maintained at 37°C using a heating coil. A constant flow of α-MEM was maintained by a constant hydrostatic pressure difference between the reservoir filled with α-MEM and the flow chamber. Three different flow rates were generated by adjusting the height difference between the tank and the microscope stage. This procedure is similar to the one outlined by DiMilla *et al.* (3). Flow rates were calculated by measuring the volume of fluid collected in 60 sec.

Before initiating flow, the number of attached cells were counted at 0.4, 0.6, 1, 1.6, and 2 cm from the center of the quartz disc in four directions 0°, 90°, 180°, and 270° (~38% of the disc area was examined during cell counts). The average of the four readings was considered as a single cell measurement. A (3.5 mm × 2.5 mm) photomask was used as a grid for counting the cells at the start of the experiment. Subsequently, flow was initiated for 5 min, and then the number of cells within each region was again recorded. Cell fractions were calculated by dividing the number of cells attached after flow by the initial number of cells attached within each region. This procedure was repeated for three different flow rates (0.4 to 2 ml/sec). A schematic of the observation scheme is shown in Fig. 3.

Shear stress at the well was determined using the following equation based on the continuity and Navier-Stokes equations [see Appendix for the derivation of this equation (Eq. A8)]:

$$\tau = \frac{3Q\mu}{4\pi h^2 r} - \frac{3\rho Q^2}{140\pi^2 h r^3}, \quad (1)$$

where τ is the shear stress at the wall, Q is the volumetric flow rate, $2h$ is the gap height between plates (0.022 cm), r is the radial distance, ρ is the density of the flowing media (~1 g/cm^3), and μ is the fluid viscosity at 37°C (0.85 cP) (19). The range of flow rates used ensured that, for $r > 0.3$ cm, laminar flow [channel Reynolds number: $2Q/(\pi\nu r) < 500$, $\nu = \mu/\rho$] existed between the upper and lower quartz discs and in the inlet tube [inlet Reynolds number: $Q/(\pi\nu R_{inlet}) < 470$] (15).

RESULTS

Morphology of Bone Cells on the Modified Surfaces

Phase-contrast light microscopy was used to observe the morphology of the bone cells on the clean, EDS, and

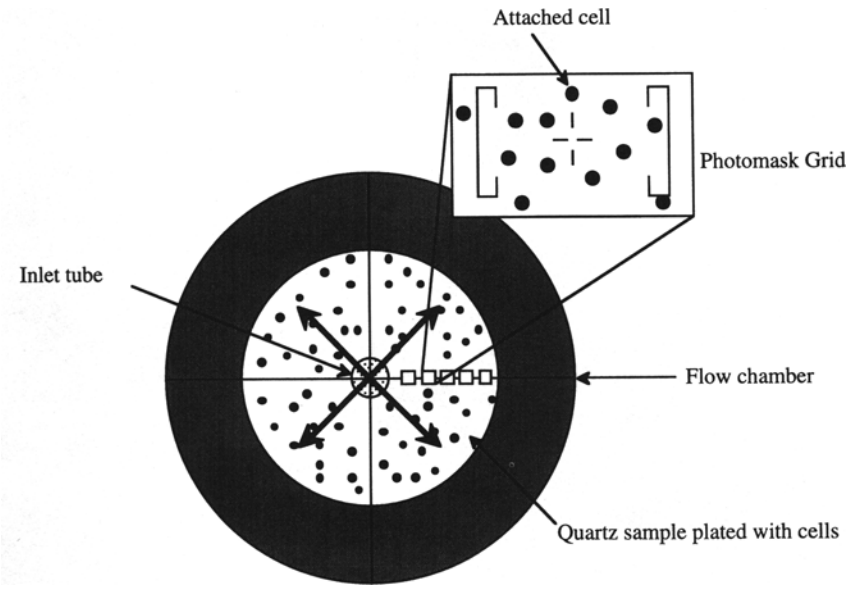

FIGURE 3. Observation scheme for the radial flow assay. Five regions (0.4 to 2 cm) were used to count the number of attached cells before and after exposure to flow.

DMS surfaces. Cells were incubated on the surfaces for either 20 min or 2 h in DMEM with 15% FBS at 37°C. Figures 4 and 5 depict the morphology of the cells on the modified quartz surfaces. Details of the image acquisition system were described elsewhere (10). A larger percentage of cells were spread at 2 hr (Fig. 5), compared with 20 min (Fig. 4) incubation. Also, for 2-hr cell incubation, the cells were more round and refractive on the DMS surfaces, compared with the flat morphology of the cells on the EDS and clean substrates. The nature of bone cell attachment and spreading on the DMS surfaces were attributed to the surface chemistry and conformation of adsorbed proteins rather than possible toxic effects caused by either the DMS layer or released DMS into the media. This was verified by incubating the cells for 24 hr in the absence of serum on patterned substrates with alternating regions of EDS/DMS. It was observed that bone cells spread both on the EDS and DMS regions. Furthermore, extended cultures of bone-derived cells on the EDS/DMS patterned substrates, in the presence of serum, exhibited proliferation of cells from the EDS onto the DMS regions (10).

Strength of Cell Attachment

Due to the heterogeneity in the strength of cell adhesion to chemically modified substrates, three different distributions (Weibull, reverse sigmoidal, and reverse log–normal) were used to analyze the relationship between surface chemistry and strength of cell adhesion. In general, as the shear stress at the wall increased, the fraction of detached cells increased. A Weibull distribution was used because it offered a probabilistic approach to data analysis. Weibull distribution compares the probability of failure as a function of applied shear stress at the wall. The reverse log–normal and reverse sigmoidal models were selected for comparison with a Weibull model and for comparison with other cell detachment studies in literature (3,30). The reverse log–normal and reverse sigmoidal models were used to fit the fraction of attached cells as a function of shear stress at the wall. The Weibull, reverse log–normal, and reverse sigmoidal distribution functions are given below:

Weibull: $W(\tau_i, m, \tau_0, \tau_u$

$$\frac{m}{\tau_0}\left(\frac{\tau_i}{\tau_0}\right)^{m-1} exp\left[-\left(\frac{\tau_i-\tau_u}{\tau_0}\right)^m\right]. \quad (2)$$

Reverselog–normal: $L(\tau_i, \mu, \sigma) =$

$$1-\frac{1}{\tau_i\sigma\sqrt{2\pi}} exp\left[\frac{-1}{2\sigma^2}(Ln(\tau_i)-\tau)^2\right]. \quad (3)$$

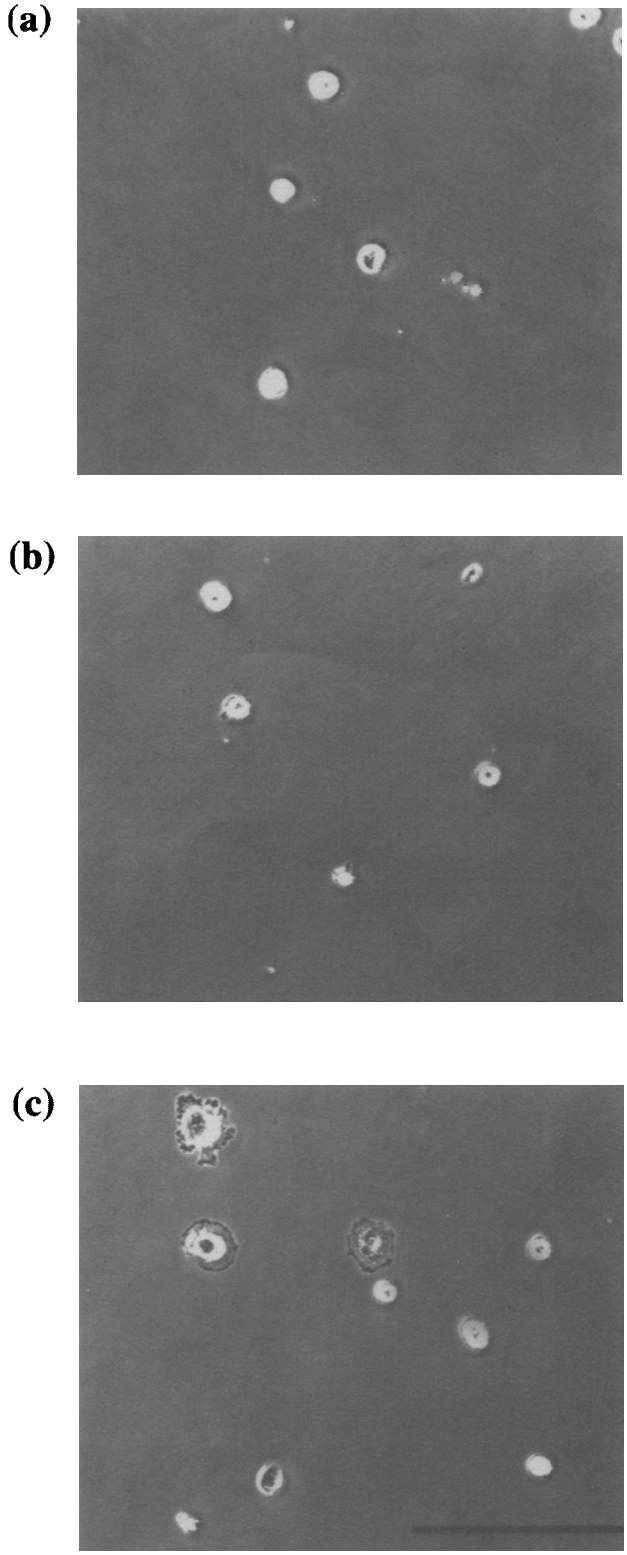

FIGURE 4. Morphology of 20-min bone cell exposure in the presence of serum to (a) clean quartz, (b) DMS, and (c) EDS surfaces. Phase-contrast light microscopy was used to take these photomicrographs at 100x. Note the larger degree of cell spreading on the EDS and clean surfaces, compared with the DMS surface. Solid bar is 250 μm in length.

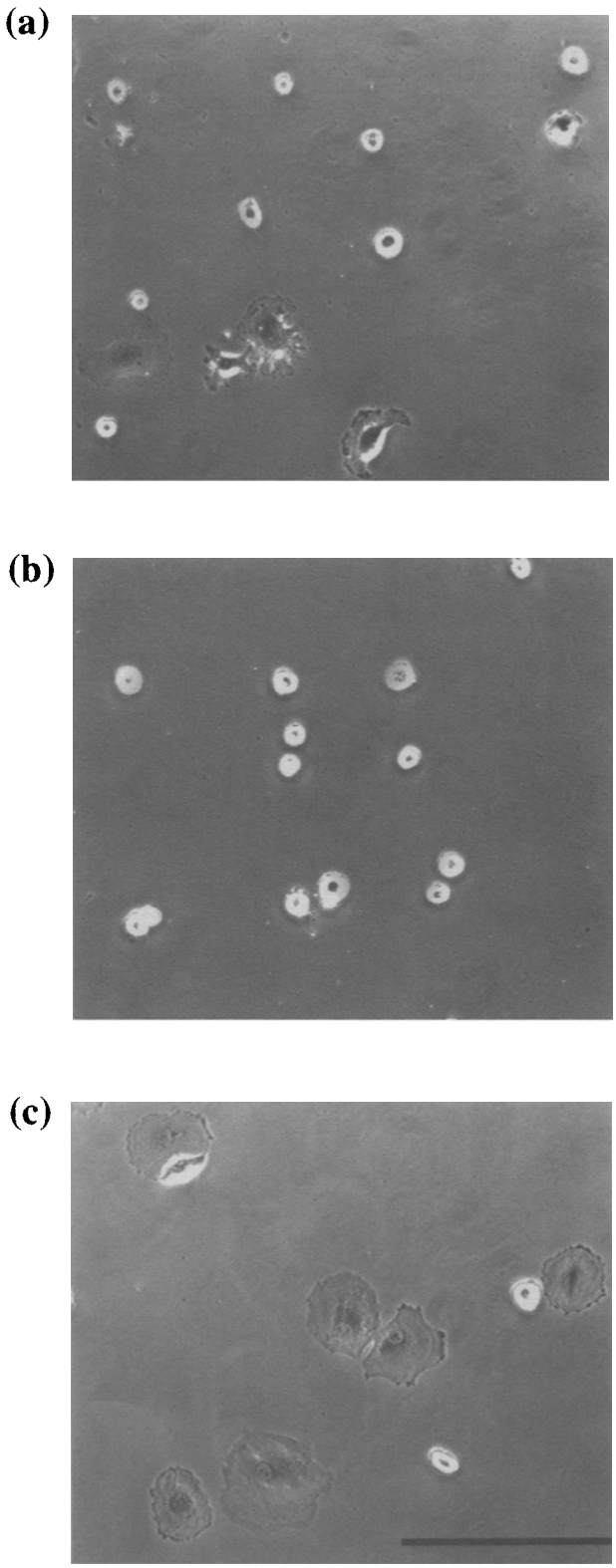

FIGURE 5. Morphology of 2-hr bone cell exposure in the presence of serum to (a) clean quartz, (b) DMS, and (c) EDS surfaces. Phase-contrast light microscopy was used to take these photomicrographs. Solid bar is 250 μm in length.

Reverse sigmoidal: $S(\tau_i, \cdot \alpha, \beta) =$

$$1 - \frac{1}{1 - exp\left[-\left(\frac{\tau_i - \alpha}{\beta}\right)\right]}. \quad (4)$$

For the Weibull distribution, m is the Weibull modulus, τ_0 is the characteristic strength (shear stress where the probability of failure is 0.632), τ_i is the shear stress at the wall (for all the models), and τ_u is the threshold stress (shear stress below which the probability of failure is 0). For the reverse log–normal distribution τ is the mean shear stress and σ is the standard deviation of the shear stress values. For the reverse sigmoidal distribution α (center parameter) is the shear stress where 50% of cells remained attached, and β is the width of transition from a high fraction to a low fraction of attached cells.

The characteristic strength of attached cells was determined in a different manner for each distribution. To use the reverse sigmoidal and reverse log–normal equations, data were arranged as fraction of cells attached to a surface as a function of applied shear stress at the wall. For the reverse sigmoidal fits, the shear stress values corresponding to a 0.5 fraction of cells attached, α, was considered as the characteristic shear strength. For the reverse log–normal fits, the median, $M = \exp(\tau)$, values were considered as the characteristic shear strength (25). The characteristic shear strength values were used to compare the effect of surface chemistry on strength of cell adhesion.

Due to the heterogeneity of shear stress values required to detach cells from surfaces, a probabilistic approach using a three-parameter Weibull distribution was chosen to analyze the data. Weibull statistics is based on the weakest link theory, which states that a material under uniform shear stress fails at the weakest point. In Weibull analysis, the parameter of interest is the characteristic strength, τ_0, which is defined as the shear stress at which the probability of cell failure is 0.632. The characteristic strength, τ_0, values were used to compare the effect of surface chemistry on the strength of bone cell adhesion. In this analysis, each cell that detached from the surface was considered as a single failure. Five regions in each quadrant of the quartz discs were used to count the number of attached cells. To ensure that no one region had a significantly higher number of attached cells, compared with other regions, the initial cell count in each region was compared using analysis of variance (ANOVA) and a Scheffé *post-hoc* comparison. If one region had a significantly higher number of cell count, a bias would have been introduced in the probability of failure values. The regions that showed a significant difference from other regions, at a level of $p < 0.05$, were not considered in the Weibull analysis. To simplify the Weibull analysis, it is a common practice to linearize Eq. 2 into the following form:

$$\underbrace{Ln\left(Ln\left(\frac{1}{1-P_i}\right)\right)}_{y} = m\underbrace{Ln(\tau_i - \tau_u)}_{x} - \underbrace{mLn(\tau_0)}_{b}, \quad (5)$$

where the left-hand side is the dependent variable (y), $\mathrm{Ln}(\tau_i - \tau_u)$ is the independent variable (x), m is the slope, and $m\ \mathrm{Ln}(\tau_0)$ is the intercept (b) of the line. To calculate P_i, the cumulative probability of cell detachment or failure at a given shear stress, an estimator was used. The estimator used in this analysis was: $P(\tau_i) = i/(N + 1)$, wherein i is the rank of ordered shear stress values, and N is the total number of cell failures. There are other estimators, such as the "median" estimator given by $P(\tau_i) = (i - 0.3)/(N + 0.4)$ (6). However, due to the large number of cells detached (*i.e.*, large N), there was no advantage of one estimator over another (6). The choice of an estimator becomes important when the size of sample is small (usually $N < 50$).

Two fitting methods, maximum likelihood (ML) and least squares (LS), were considered for calculating the three parameters (m, τ_u, and τ_0) in the Weibull distribution. The ML method was considered to be superior to the LS method because, in Weibull distributions, a logarithmic scale is used that spreads the smallest shear stress values more than the larger stress values. For LS fitting methodology, the smallest shear stress values have a larger influence on the slope, compared with the ML method. Thus, the LS method can lead to larger errors in estimating the Weibull parameters m, τ_0, τ_u. All of the data were fitted using the ML method. The ML estimation technique used in this study was modeled after techniques developed by Sonderman *et al.* (26) and Thoman *et al.* (28). Figure 6 summarizes the steps involved in the Weibull analysis. Table 1 summarizes the parameters obtained for the Weibull distribution.

Figures 7 and 8 show reverse sigmoidal and reverse log–normal fits for 20 min and 2 hr bone cell incubation on the substrates, respectively. Figure 9 shows representative Weibull plots for 20 min and 2-hr cell incubation on the substrates. On the Weibull plots, the characteristic shear strength is the point at which the Weibull line intersects the 0.632 probability of failure. The characteristic shear strength was used as the parameter for comparing the effect of surface chemistry on strength of cell adhesion. In addition to the characteristic strength values, the Weibull threshold strength and the modulus were also compared for each surface. ANOVA and Scheffë *post-hoc* comparison was used to compare the parameters of the three models for each surface. As shown in Table 1, for 20 min of cell incubation, the magnitude of Weibull modulus was significantly higher ($p < 0.04$) on the EDS and clean surfaces, compared with the DMS surfaces. However,

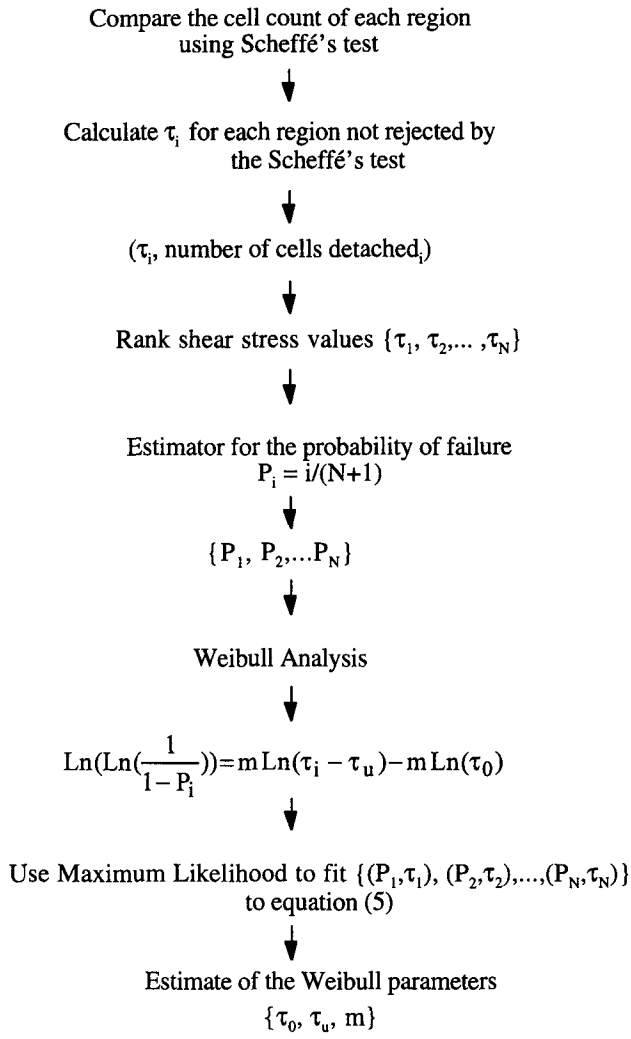

FIGURE 6. Summary of steps involved in using Weibull distribution to estimate the characteristic strength of bone cells to modified substrates.

within 2 hr of cell incubation, there was no statistically significant difference between the Weibull modulus of the three surfaces. The Weibull threshold strength values exhibited no correlation with the surface chemistry and pe-

TABLE 1. Summary of parameters used in the Weibull distribution

Fitting Models	Clean ($n = 3$)	EDS ($n = 3$)	DMS ($n = 3$)
Weibull model (20 min)			
Weibull modulus (m)	1.6 ± 0.3	1.7 ± 0.2	1.2 ± 0.2
Threshold stress (τ_u, dyne/cm^2)	8 ± 3	7 ± 1	5 ± 1
Weibull model (2 hr)			
Weibull modulus (m)	1.6 ± 0.3	1.9 ± 0.4	1.7 ± 0.3
Threshold stress (τ_u, dyne/cm^2)	8 ± 2	7 ± 3	8 ± 2

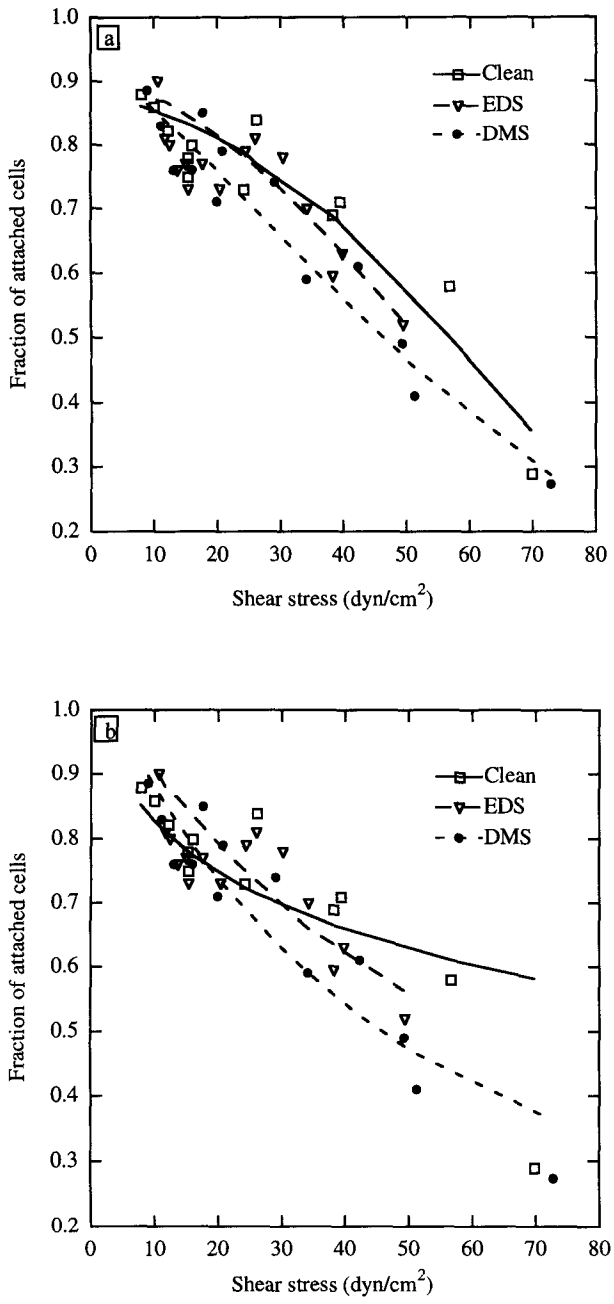

FIGURE 7. Fraction of attached cells to EDS, DMS, and clean substrates for 20-min cell incubation in the presence of serum. Reverse sigmoidal (a) and reverse log–normal (b) distributions were used to fit the data. The fraction of attached cells was calculated by dividing the number of attached cells after exposure to flow by the initial number of attached cells with no exposure to shear stress. The number of attached cells were counted after 5 min of exposure to flow.

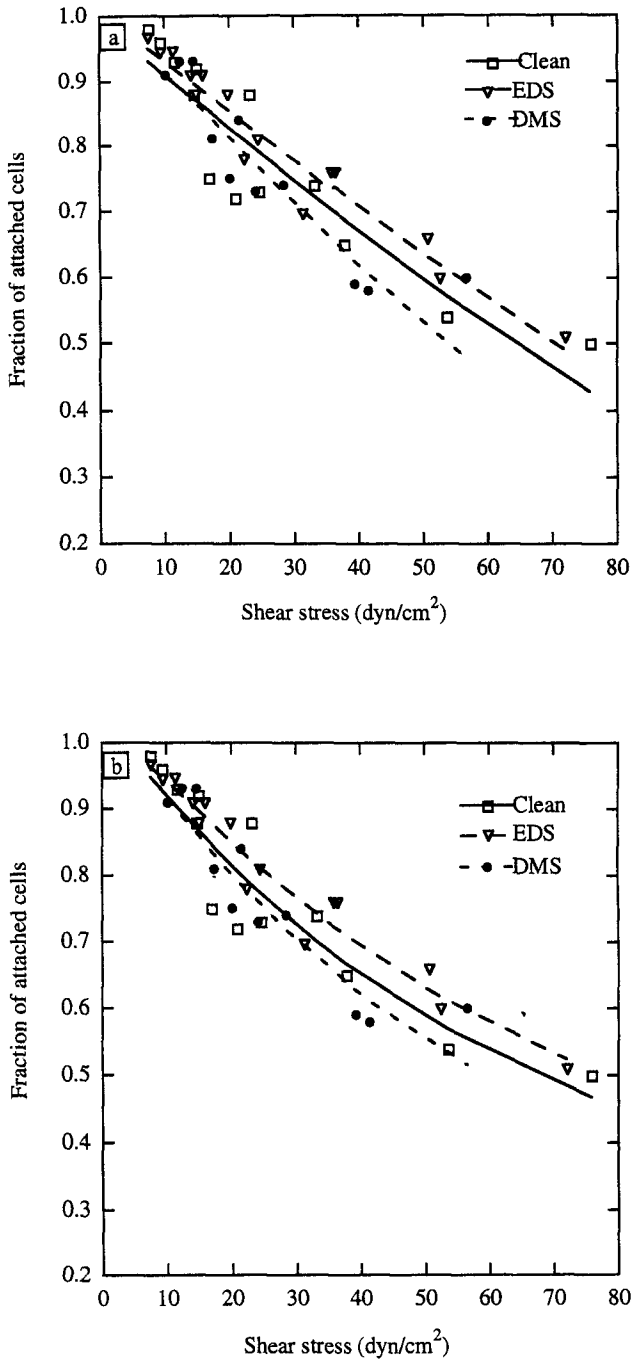

FIGURE 8. Fraction of attached cells to EDS, DMS, and clean substrates for 2-hr cell incubation in the presence of serum. Reverse sigmoidal (a) and reverse log–normal (b) distributions were used to fit the data.

riod of cell incubation. Such an indifference was attributed to the relatively few number of cells detaching (<4 to 5% of the number of cells attached) at low shear stress values (*i.e.*, $\tau_i < 10$ dyne/cm^2).

Figure 10 compares the characteristic parameter for the Weibull, reverse sigmoidal, and reverse log–normal distributions for 20-min and 2-hr cell incubations on the surfaces. Regardless of the model used, within 20 min of cell incubation, there was a statistically significant difference ($p < 0.001$) between the characteristic strength of adhesion to EDS and DMS surfaces, with EDS having a higher characteristic strength. However, the reverse sigmoidal, and reverse log–normal distributions showed no signifi-

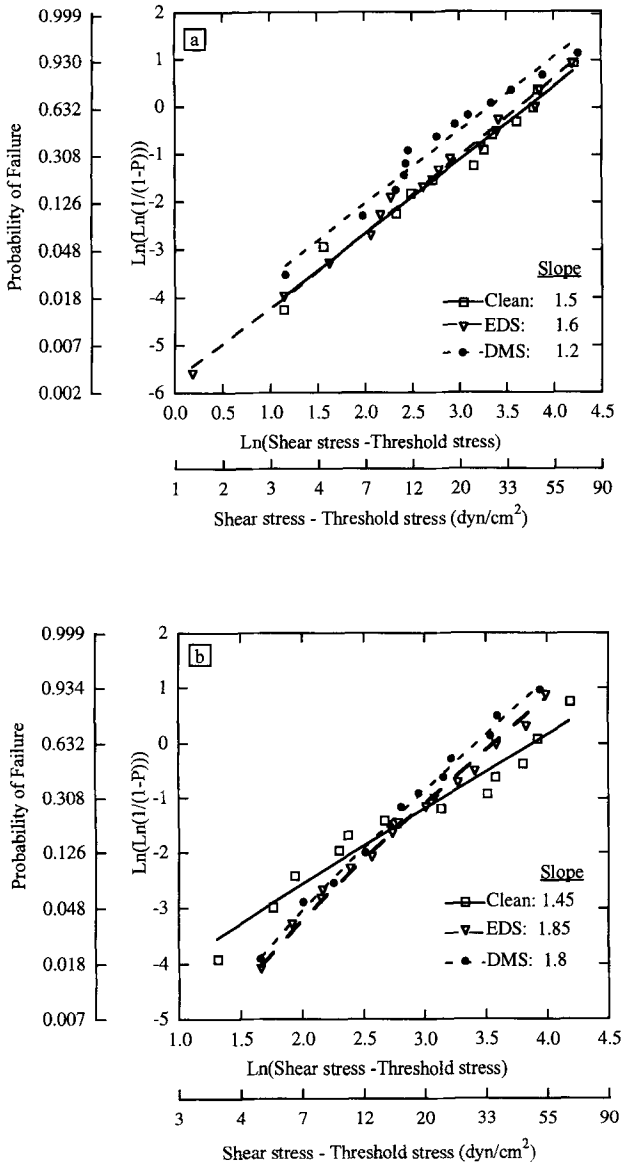

FIGURE 9. Representative three-parameter Weibull probability plots for 20 min (a) and 2 hr (b) of cell incubation on the EDS, DMS, and clean substrates. ML fitting was used to estimate the parameters of the Weibull distribution. The parameter of interest is the characteristic strength that is defined as the shear strength at a 0.632 probability of failure. Small differences in the Weibull modulus, slope, led to large differences in the characteristic strength.

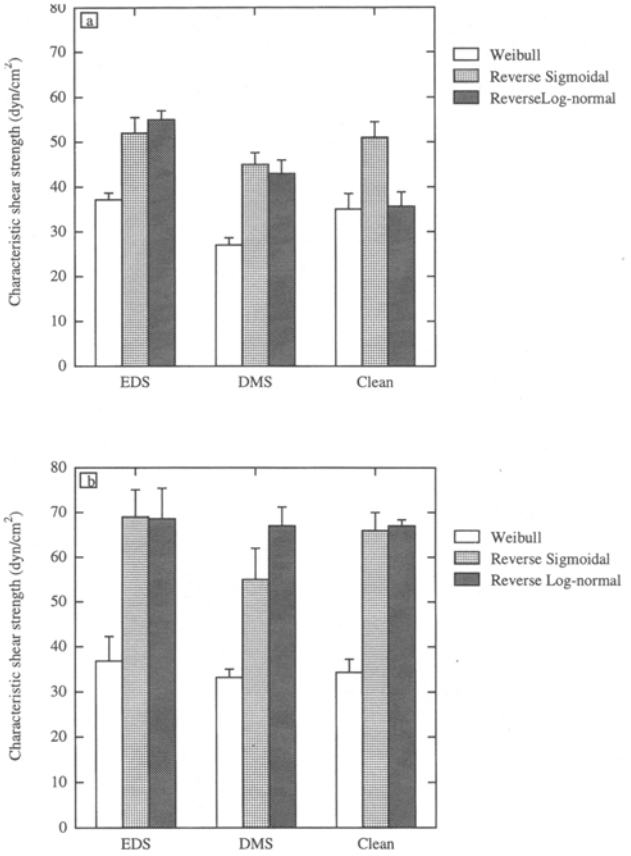

FIGURE 10. Comparison of the characteristic shear strength of Weibull, reverse sigmoidal, and reverse log–normal distributions. For 20-min cell incubation (a), there was a statistical significant difference ($p < 0.001$) between the characteristic shear strength of EDS and DMS surfaces. For 2-hr cell incubation (b), there was no significant difference between the characteristic strength of the EDS, DMS, and clean surfaces. Note that the characteristic strength for 2-hr cell exposure was larger than 20-min cell incubation. Due to the complex distribution of the shear strength values, the Weibull distribution was considered to be more representative of the shear strength data.

cant difference between the DMS and clean surfaces, whereas the Weibull fit showed a statistical significance between the DMS and clean surfaces ($p < 0.001$). For 2-hr cell incubation, none of the fitting models exhibited a significant difference between the characteristic shear strength of the EDS, DMS, and clean surfaces. For both 20-min and 2-h cell incubation, the magnitude of the characteristic strength for the reverse sigmoidal, and reverse log–normal fits was larger than the Weibull fit.

DISCUSSION

In previous studies, we have demonstrated that, within 30 min of incubation on a EDS/DMS patterned surface, in the presence of serum, bone cells preferentially distributed on amine-terminated, EDS regions (10). In an effort to understand better the mechanism of cell organization on patterned substrates, we investigated whether bone cell arrangement on amine regions of the EDS/DMS pattern was adhesion mediated. Weibull, reverse sigmoidal, and reverse log–normal distributions were used to examine the adhesive nature of the EDS, DMS, and unmodified clean quartz substrates (control surfaces). There was a wide variation in strength of adhesion for a cell population, possibly caused by differences in the surface density of ligands, density of ligand-receptor bonds, the area of focal

contracts, the number of focal contacts, cell type, and the area of spread cells (2,24). Such variations resulted in a range of shear stresses required to detach a population of cells from a substrate. Thus, for a complex shear strength distribution, the characteristic parameters obtained from a shear stress analysis, which uses a probabilistic approach, was considered to be more representative of the adhesion strength of a cell population, compared with reverse sigmoidal, and reverse log–normal distributions. Thus, in this study, we base our discussions and conclusions on the results obtained from Weibull analysis.

Within 20 min of cell incubation, the surface chemistry dictates the strength of cell adhesion in the presence of serum through an intermediary layer of adsorbed proteins. Spectroscopic ellipsometry results indicated that the thickness of adsorbed proteins, from media containing serum, was equal on homogeneous surfaces with either EDS or DMS overlayers (10). Recently, we have used immunofluorescent staining and confocal microscopy to show that the preferential attachment of normal rat osteoblasts and human-derived bone cells to the EDS regions was dependent on the adsorption of vitronectin from serum onto the EDS regions of a EDS/DMS patterned surface (data not shown) (18). Adsorption of vitronectin was localized within the EDS regions defined by surface analysis (*i.e.*, time-of-flight secondary ion mass spectrometry). Bone cells were not spatially distributed on EDS/DMS patterned substrates when vitronectin was depleted from serum; however, the removal of fibronectin from complete serum did not significantly change the cell distribution observed (29). Based on these experiments, we believe the differences in the strength of cell adhesion measured reflects the interaction of primary bone cells with adsorbed vitronectin for EDS and clean surfaces, and the absence of vitronectin on DMS surfaces. Neither the surface density nor the surface conformation of active vitronectin on EDS or clean surfaces are known at this time.

The role of endogenous proteins in masking the surface chemistry may explain the indifference, within 2 hr of cell incubation, in the strength of cell adhesion to the EDS, clean, and DMS surfaces. The major extracellular protein secreted by osteoblast-like cells is type I collagen (21). Various *in vivo* and *in vitro* studies have shown that the rate of collagen synthesis and release by osteoblast-like cells was within 36 to 60 min (31). Investigators studying the secretion rate of noncollagenous proteins, such as phosphoproteins, have found secretion rates to be within 15 to 30 min, and determined that the rate of phosphoprotein and collagen type I secretion (45 to 60 min) were different (4). It is not clear that, *in vitro,* the same time periods are required for secretion of endogenous proteins by osteoblasts derived from primary cultures. However, these results tend to support our hypothesis that 20 min of cell incubation is not sufficient for significant secretion and activation of endogenous proteins; but, 2 hr is sufficient time for significant secretion of collagen and noncollagenous proteins onto the surfaces by cells. Presumably, the cells use these endogenous proteins when interacting with the material surface (*e.g.*, DMS).

Due to the heterogeneity of the strength of cell attachment, a probabilistic analysis (Weibull distribution) was considered to be more representative of the complex cell-substratum adhesion strength, as opposed to the deterministic analyses, reverse sigmoidal and reverse log–normal. As depicted in Fig. 10a, only the Weibull model predicted that, for 20 min of cell incubation, there was a statistically significant difference between the adhesion strength of bone cells on the DMS and clean surfaces. This observation was consistent with our previous findings that bone cell organization was observed on clean regions of a patterned substrate with alternating regions of DMS and clean chemistries (10). These observations indicated that, compared with reverse sigmoidal and reverse log–normal distributions, the predictions of the Weibull model were more consistent with experimental observations.

There are other additional advantages of using the Weibull distribution. The Weibull distribution can predict if competing mechanisms that lead to cell failure exist. For example, a multimodal Weibull distribution can indicate whether cell detachment is due to different competing mechanisms of cell failure or different subpopulations of cells exhibiting different adhesion strengths (5). In this study, a bimodal Weibull distribution was considered for data analysis. The bimodal approach was initially chosen to establish different mechanisms of cell failure, such as membrane rupture or breaking of receptor–ligand bonds. Regardless of the type of surface chemistry and period of cell incubation, few of the experiments exhibited a bimodal distribution, and the bimodal distribution showed no correlation with time of cell incubation and type of surface chemistry. Thus, the bimodal approach seemed inconsistent and was not used to compare the effect of surface chemistry on the strength of cell adhesion. A three-parameter Weibull distribution was selected because it is the general form of a Weibull distribution. In many studies, the threshold stress is assumed to be 0; therefore, the three-parameter form of Weibull reduces to a two-parameter (*i.e.*, characteristic strength and Weibull modulus) distribution. The probabilistic approach has disadvantages too. For example, in a Weibull distribution, there has to be a large number of samples, or cell detachments, to obtain low uncertainty in the Weibull parameters. In this study, after exposure to flow, an average of 500 cells detached from a surface; this resulted in an uncertainty of ±20% for the Weibull modulus, ±10% for the characteristic shear strength, and ±30% for the threshold shear strength. These uncertainty values were obtained from a study conducted by Duffy *et al.* (5), who used a Monte

Carlo simulation to generate the uncertainty values in the Weibull parameters.

In this study, we have referred to the shear stress at the wall (Eq. 1) as the adhesion strength of cells to the surfaces; however, the force exerted on a cell depends not only on the flow rate, viscosity of media, density of media, and geometry of the flow chamber, but also on the shape of the cell. Olivier and Truskey (24) conducted a numerical study to examine the effect of endothelial cell shape on the drag force and torque on a cell. The result of the study showed that the drag force and torque decreased by a factor of 2 and 20, respectively, during cell spreading. Therefore, one needs to use caution when citing the shear stress at the wall as the strength of cell adhesion. To obtain a better estimate of the strength of cell adhesion, one needs to consider the contact area, the number of ligand–receptor interactions, the rate of receptor diffusion into a contact area, the density of ligand–receptor interactions in the regions of focal contact, the force required to break a ligand–receptor bind, and a model that includes all of these parameters (14,32). The lack of a model that can fully incorporate all of the previously described variables makes the use of shear stress at the wall, that causes cell detachment, an incomplete but adequate estimate of the strength of cell attachment to chemically and biologically modified surfaces.

Understanding the mechanisms involved in cell adhesion and detachment is of considerable interest in engineering biomaterial surfaces that promote or diminish cell attachment. Numerical and empirical studies on the detachment of mammalian cells from model surfaces have identified two mechanisms of detachment: pulling receptors through the cell membrane and (or) breaking the receptor–ligand bond (8,30,32). Immunofluorescence and interference reflection microscopy analyses have been used to reveal the role of focal adhesion sites on strength of cell adhesion and spreading (30). We did not attempt to identify the mechanisms of cell, detachment, but did qualitatively observe that both modes of failure occur with our cells and surfaces. Regardless of the model used for data analysis, the processed data did not manifest any consistent trends toward the presence of different mechanisms of cell detachment. Furthermore, the degree of cell spreading for 2 hr of cell incubation on the EDS, clean, and DMS surfaces did not correspond to the strength of cell adhesion. Although a larger percentage of cell spreading was observed on the EDS and clean surfaces, compared with the DMS surfaces (see Fig. 5 and 6), the Weibull characteristic strength values for these surfaces were not statistically different. Studies by Truskey and Proulx (30) and Horbett *et al.* (11) also showed that a higher degree of cell spreading did not result in a higher measured shear stress for cell detachment. Truskey and Proulx offered the explanation that the bond density (*i.e.*, number of receptor–ligand bonds) in the contact area between the cell and surface is the critical factor controlling the strength of cell adhesion. We propose that, in our cell adhesion experiments, the bond density in the contact area was similar on EDS, DMS, and clean surfaces for 2 hr of cell incubation. We did not attempt to quantify the bond density in the contact areas, because the objectives of this study were to develop a rapid cell detachment assay, introduce a novel probabilistic method of data analysis, and use the prediction of the model to explain our cell patterning experiments rather than elucidate the mechanisms of cell adhesion.

CONCLUSIONS

A novel probabilistic approach (Weibull statistics) was used to assess the differences in normal rat bone cell attachment strengths to materials with modified surface chemistry. After 20-min incubation attachment strengths were significantly larger on EDS and clean substrates, compared with DMS surfaces. Differences in attachment strengths were mediated by an intermediary layer of adsorbed proteins, wherein vitronectin was preferentially adsorbed to EDS and clean surfaces. Within 2 hr of cell exposure, surface chemistry had no significant effect on the strength of bone cell adhesion. Results of this study suggest that the mechanism of bone cell distribution on amine-terminated regions of a patterned EDS/DMS substrate was adhesion mediated. Synthesis of endogenous proteins by bone cells was proposed to be responsible for masking the effect of surface chemistry on the strength of cell adhesion within 2 hr of cell incubation.

REFERENCES

1. Baier, R. E. Adhesion in biological systems. In: Surface properties influencing biological adhesion, edited by R. S. Manly, New York: Academic Press, 1970, pp. 15–45.
2. Cozens-Roberts, C., J. A. Quinn, and d. A. Lauffenberger. Receptor-mediated adhesion phenomena: model studies with the radial flow detachment assay. *Biophys. J.* 58:107–125, 1990.
3. DiMilla, P. A., J. A. Stone, S. M. Albelda, D. A. Lauffenburger, and J. A. Quinn. Measurement of cell adhesion and migration on protein-coated surfaces. *Mater. Res. Soc. Symp. Proc.* 252:205–212, 1992.
4. DiMuzio, M. T., and A. Veis. The biosynthesis of phosphophoryns and dentin collagen in the continuously erupting rat incisor. *J. Biol. Chem.* 253:6845–6852, 1978.
5. Duffy, S. F., L. M. Powers, and A. Starlinger. Reliability analysis of structural ceramic components using a three-parameter Weibull distribution. *J. Eng. Gas Turbines Power* 115:109–116, 1993.
6. Faucher, B., and W. R. Tyson. On the determination of Weibull parameters. *J. Mater. Sci. Lett.* 23:1199–1203, 1988.
7. Fryer, P. J., N. K. H. Slater, and J. E. Duddridge. Sugges-

tions for the operation of radial flow cells in cell adhesion and biofouling studies. *Biotech. Bioeng.* 27:434–438, 1985.
8. Hammer, D. A., and D. A. Lauffenburger. A dynamical model for receptor-mediated cell adhesion to surfaces. *Biophys. J.* 52:475–487, 1987.
9. Healy, K. E., B. Lom, and P. E. Hockberger. Spatial distribution of mammalian cells dictated by materials surface chemistry. *Biotech. Bioeng.* 43:792–800, 1994.
10. Healy, K. E., C. H. Thomas, A. Rezania, J. E. Kim, P. J. McKeown, B. Lom, and P. E. Hockberger. Kinetics of bone cell organization and mineralization on materials with patterned surface chemistry. *Biomaterials* 16:195–208, 1995.
11. Horbett, T. A., J. J. Waldburger, B. D. Ratner, and A. S. Hoffman. Cell adhesion to a series of hydrophilic-hydrophobic copolymers studied with a spinning discs apparatus. *J. Biomed. Mater. Res.* 22:383–404, 1988.
12. Hubbell, J. A., S. P. Massia, and P. D. Drumheller. Surface-grafted cell-binding peptides in tissue engineering of the vascular graft. *N.Y. Acad. Sci.* 655:253–258, 1992.
13. Kleinfeld, D., K. H. Kahler, and P. E. Hockberger. Controlled outgrowth of dissociated neurons on patterned substrates. *J. Neurosci.* 11:4098–4120, 1988.
14. Kuo, S. C., and D. A. Lauffenberger. Relationship between receptor/ligand binding affinity and adhesion strength. *Biophys. J.* 65:2191–2200, 1993.
15. Livesey, J. L. Inertia effects in viscous flow. *Int. J. Mech. Sci.* 1:84–88, 1960.
16. Lom, B., K. E. Healy, and P. E. Hockberger. A versatile technique for patterning biomolecules onto glass coverslips. *J. Neurosci. Methods* 50:385–397, 1993.
17. Massia, S. P., and J. A. Hubbell. Covalent surface immobilization of Arg-Gly-Asp- and Tyr-Ile-Gly-Ser-Arg-containing peptides to obtain well-defined cell-adhesive substrates. *Analyt. Biochem.* 1987:292–301, 1990.
18. McFarland, C. D., C. H. Thomas, K. E. Healy, M. L. Jenkins, and J. G. Steele. The role of serum glycoproteins in determining the spatial organisation of bone cells on patterned surfaces. 5th World Congress on Biomaterials, Toronto, Ontario, Canada, 1996, p. 129.
19. McQueen, A., and J. E. Bailey. Influence of serum level, cell line, flow type and viscosity on flow-induced lysis of suspended mammalian cells. *Biotech. Lett.* 11:531–536, 1989.
20. Moller, P. S. Radial flow without swirl between parallel discs. *Aeronaut. Q.* 14:163–186, 1963.
21. Morris, N. P., L. I. Fessler, A. Weinstock, and J. H. Fessler. Procollagen assembly and secretion in embryonic chick bone. *J. Biol. Chem.* 250:5719–5726, 1975.
22. Morrissey, B. W. The adsorption and conformation of plasma proteins: a physical approach. *Ann. N.Y. Acad. Sci.* 283:50–64, 1977.
23. Narasimhan, C., and C. S. Lai. Conformational changes of plasma fibronectin detected upon adsorption to solid substrates: a spin-label study. *Biochemistry* 28:5041–5046, 1989.
24. Olivier, L. A., and G. A. Truskey. A numerical analysis of forces exerted by laminar flow on spreading cells in a parallel plate flow chamber assay. *Biotech. Bioeng.* 42:963–973, 1993.
25. Selvin, S., and S. M. Rappaport. A note on the estimation of the mean value from a lognormal distribution. *Am. Ind. Hyg. Assoc. J.* 50:627–630, 1989.
26. Sonderman, D., K. Jakus, J. E., Ritter, Jr., S. Yuhaski, Jr., and T. H. Service. Maximum likelihood estimation techniques for concurrent flow subpopulations. *J. Mater. Sci.* 20:207–212, 1985.
27. Sukenik, C. N., N. Balachander, L. A. Culp, K. Lewandowska, and K. Merritt. Modulation of cell adhesion by modification of titanium surfaces with covalently attached self-assembled monolayers. *J. Biomed. Mater. Res.* 24: 1307–1322, 1990.
28. Thoman, D. R., L. J. Bain, and C. E. Antle. Inferences on the parameters of the Weibull distribution. *Technometrics* 11: 445–460, 1969.
29. Thomas, C. H., C. D. McFarland, M. L. Jenkins, A. Rezania, J. A. Steele, and K. E. Healy. The role of vitronectin in the attachment and spatial distribution of bone-derived cells on materials with patterned surface chemistry. *J. Biomed. Materials Res.*, in press, 1997.
30. Truskey, G. A., and T. L. Proulx. Relationship between 3T3 cell spreading and the strength of adhesion on glass and silane surfaces. *Biomaterials* 14:243–259, 1993.
31. Vuust, J., and K. A. Piez. A kinetic study of collagen biosynthesis. *J. Biol. Chem.* 247:856–862, 1972.
32. Ward, M. D., M. Dembo, and D. A. Hammer. Kinetics of cell detachment: effect of ligand density. *Ann. Biomed. Eng.* 23:322–331, 1995.

APPENDIX

This appendix focuses on the theoretical approaches used in characterizing the actual flow between parallel discs. The most extensive study on radial flow between parallel discs have been conducted by Moller (20). Also, Fryer *et al.* (7) has pointed to some problems with the assumptions used in deriving the velocity profile between the parallel discs. In an effort to expand on Fryer's work, we present a more rigorous approach to the use of the equations describing the velocity profile between parallel discs and shear stress at the wall.

Derivation of Equation of Motion for Laminar Radial Flow Between Parallel Discs

Velocity and pressure profiles of any flow can be characterized by considering the continuity and Navier-Stokes equations. Assuming a radial (u_θ and u_z are zero), incompressible, and steady-state flow between two parallel discs, the continuity and momentum equations (in cylindrical coordinates) reduce to the following forms (see Fig. A1):

$$\frac{\partial u_r}{\partial r} + \frac{u_r}{r} = 0 \tag{A1}$$

$$\rho u_r \frac{\partial u_r}{\partial r} = -\frac{dp}{dr} + \mu \left(\frac{\partial^2 u_r}{\partial r^2} + \frac{\partial u_r}{r \partial r} - \frac{u_r}{r^2} + \frac{\partial^2 u_r}{\partial z^2} \right), \tag{A2}$$

where u_r is the velocity profile, r is the radial distance from the center of the disk, ρ is the fluid density, μ is the fluid viscosity, and p is the static pressure. By substituting Eq. A1 into A2, the equation of motion reduces to the following form:

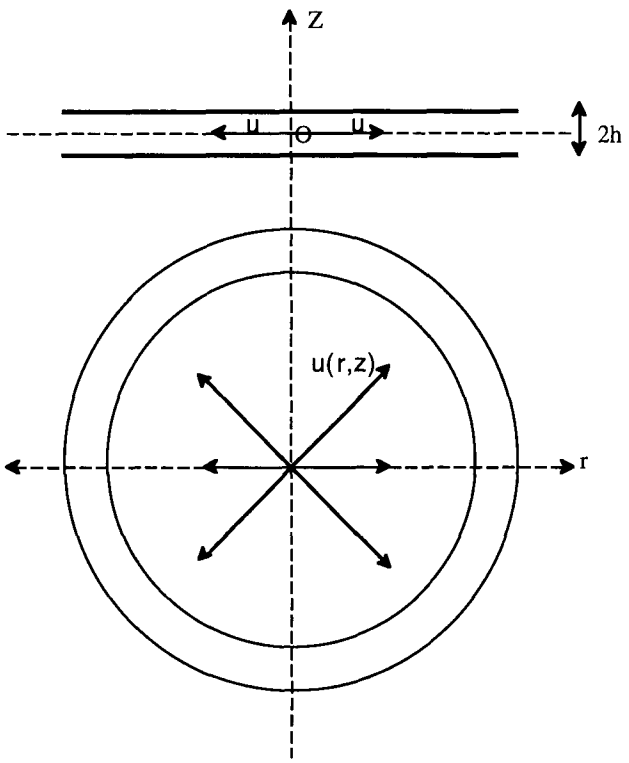

FIGURE A1. Schematic of radial flow between parallel plates (u_r: velocity in r direction; $2h$: gap between parallel discs).

$$-\rho \frac{u_r^2}{r} = -\frac{dp}{dr} + \mu \frac{\partial^2 u_r}{\partial z^2}. \tag{A3}$$

The first term is the inertia term, the second term is the pressure term, and the last term is the viscous term. Omission of the inertia term leads to the creeping flow or Reynolds equation. It is not possible to integrate directly Eq. A3 unless the nonlinear term is omitted. One method to solve Eq. A3 is to assume a velocity profile and then integrate the equation to solve for the velocity profile (15). Also, numerical integration and series solution techniques have been used as alternative approaches to solve Eq. A3 (7). It is a common practice to approximately a nonlinear term in a differential equation by substituting it with a linear term. For example, a parabolic velocity profile $u_r(z) = 3Q(h_2 - z^2)/8\pi r h^3$ (Q is the volumetric flow rate) can be substituted for the velocity in the inertia term and the resulting equation integrated twice yielding the following velocity profile:

$$u_r(z) =$$

$$\frac{1}{2\mu}\frac{dp}{dr}(z^2 - h^2) - \frac{9Q^2\rho}{64\mu\pi^2 r^3 h^6}\left(\frac{z^6}{30} - \frac{h^2 z^4}{6} + \frac{h^4 z^2}{2} - \frac{11h^6}{30}\right). \tag{A4}$$

$$u_r(+h) = 0$$

$$u_r(-h) = 0.$$

Noting that the volume flow rate (from the continuity equation and assuming symmetry about z = 0) is:

$$Q = 4\pi r \int_0^h u_r \, dz \tag{A5}$$

and by inserting Eq. A4 and A5 the pressure gradient is obtained

$$\frac{dp}{dr} = \frac{-3Q\mu}{4\pi r h^3} + \frac{27\rho Q^2}{280\pi^2 r^3 h^2}. \tag{A6}$$

by substituting Eq. A6 into A4, the following velocity profile is obtained

$$u_r(z) =$$

$$\frac{3Q(h^2 - z^2)}{8\pi r h^3} - \frac{9Q^2\rho}{64\pi^2\mu r^3 h^6}\left(\frac{z^6}{30} - \frac{h^2 z^4}{6} + \frac{11h^4 z^2}{70} - \frac{h^6}{42}\right). \tag{A7}$$

The first term of Eq. A7 is the parabolic velocity profile due to the viscous effects, and the second term is due to the inertia effects in the momentum equation. The shear stress at the wall (z = −h) is obtained by differentiating Eq. A7 and multiplying it by the fluid viscosity

$$\tau_{wall} = \mu \frac{\partial u}{\partial z} = \frac{3Q\mu}{4\pi r h^2} - \frac{3\rho Q^2}{140\pi^2 r^3 h}. \tag{A8}$$

Some of the other shear stress approximations given in the literature are as follows:

(a) An approximation solution was obtained by Moller, who assumed a parabolic shape for the velocity profile and used an integral momentum approach to solve for the shear stress at the wall (20):

$$\frac{dp}{dr} = -\frac{3Q\mu}{4\pi r h^3} + \frac{27Q^2\rho}{300\pi^2 h^2 r^3} \tag{A9}$$

$$\tau_{wall} = \frac{3Q\mu}{4\pi r h^2} - \frac{3Q^2\rho}{200\pi^2 r^3 h}. \tag{A10}$$

(b) Peube (7), is this case a power series solution to Eqs. A1 and A2, was obtained:

$$\tau_{wall} = \frac{3Q\mu}{4\pi r h^2} - \frac{0.0022\rho Q^2}{r^3 h} - \frac{0.01\rho Q^2 h}{r^5} - \frac{0.00006\rho^2 Q^3}{\mu r^5} + \frac{0.00003\rho^2 Q^2 h^3}{\mu^2 r^5}. \tag{A11}$$

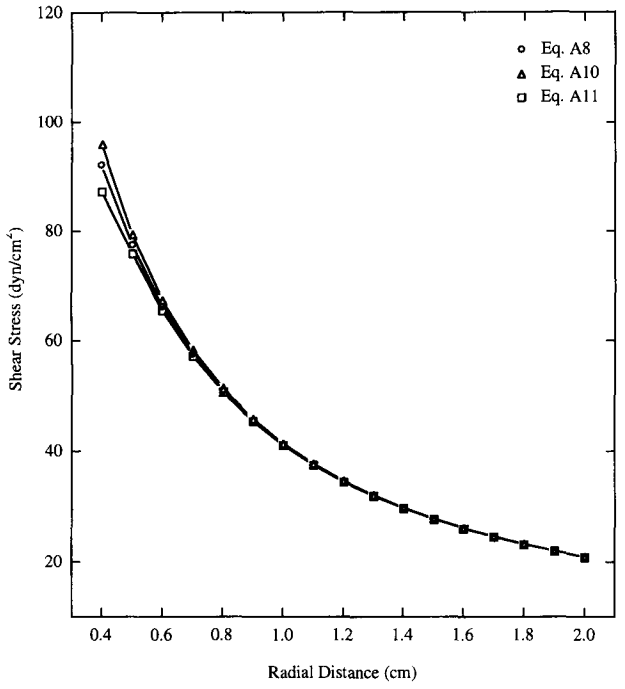

FIGURE A2. Comparison of shear stress profiles given by Eqs. A8, A10, and A11 for Q = 2 ml/sec, h = 0.011 cm, μ = 0.85cP, and ρ = 1 g/cm^3. For r > 0.4 cm, there is little difference (~10% at r = 0.4 cm) between the shear stress profiles.

Figure A2 shows the shear stress profiles (τ_{wall}) of Eqs. A8, A10, and A11. For the smallest radial distance used in this study, r = 0.4 cm, the magnitude of the shear stress profiles (Eqs. A8, A10, and A11) are within ~10% of each other.

The significance of the inertia term in Eq. A3 can be evaluated by considering an order of magnitude comparison between the inertia and viscous terms in Eq. A3:

$$O\left|\rho u \frac{\partial u}{\partial r}\right| = Q\left|\mu \frac{\partial^2 u}{\partial z^2}\right|$$

$$\left(\rho \frac{Uh}{\mu}\right) = \left(\frac{R}{h}\right)$$

$$\mathrm{Re} = \left(\frac{R}{h}\right).$$

If the magnitude of the Reynolds number [$2\rho Q/(\pi\mu r)$ < 500 for the experimental conditions in this study] is of the same order of magnitude as the aspect ration (R/h ~ 180 for the geometry of the RFA), the inertia terms cannot be omitted from Eq. A3. However, if the Reynolds number is at least an order of magnitude smaller than the aspect ratio, the inertia term can be omitted from Eq. A3.

Note that the equations listed herein are valid for a laminar flow regime, so care should be taken to avoid radial distances and inlet flow rates that leads to a turbulent flow regime (Reynolds number > 2,000). In this study, the range of inlet flow rates (0.2 to 2 ml/sec) and radial distances (r > 0.3 cm) ensured a Reynolds number < 500, thus indicating a laminar flow regime.

NOMENCLATURE

EDS = *N*-(2-aminoethyl)-3-aminopropyl-trimethoxysilane
DMS = dimethyldichlorosilane
τ, τ_i = shear stress at the wall (dyne/cm^2)
Q = volumetric flow rate (ml/sec)
μ = absolute viscosity (cP)
h = gap height (cm)
ρ = density (g/cm^3)
r = radial distance (cm)
ν = kinematic viscosity (cm^2/sec)
m = Weibull modulus
τ_0 = characteristic strength for Weibull model (dyne/cm^2)
τ_ν = threshold stress for Weibull model (dyne/cm^2)
σ = standard deviation for reverse log–normal model (dyne/cm^2)
τ = mean shear stress for reverse log–normal model (dyne/cm^2)
α = center parameter for reverse sigmoidal model (dyne/cm^2)
β = width parameter for reverse sigmoidal model (dyne/cm^2)
P_i = probability of failure
u = velocity profile (cm/sec)
P = pressure profile (dyne/cm^2)
R = radial distance (2 cm)
Re = Reynolds number
R_{inlet} = radius of the inlet tube (cm)